Dynamic scaling and quasiordered states in the two-dimensional Swift-Hohenberg equation

K. R. Elder
Department of Physics, McGill University, Rutherford Building, 3600 University Street, Montréal, Québec, Canada H3A 2T8

Jorge Viñals
Supercomputer Computations Research Institute, B-186, Florida State University, Tallahassee, Florida 32306-4052

Martin Grant
Department of Physics, McGill University, Rutherford Building, 3600 University Street, Montréal, Québec, Canada H3A 2T8
(Received 26 May 1992; revised manuscript received 19 August 1992)

The process of pattern formation in the two-dimensional Swift-Hohenberg equation is examined through numerical and analytic methods. Dynamic scaling relationships are developed for the collective ordering of convective rolls in the limit of infinite aspect ratio. The stationary solutions are shown to be strongly influenced by the strength of noise. Stationary states for small and large noise strengths appear to be quasiordered and disordered, respectively. The dynamics of ordering from an initially inhomogeneous state is very slow in the former case and fast in the latter. Both numerical and analytic calculations indicate that the slow dynamics can be characterized by a simple scaling relationship, with a characteristic dynamic exponent of $\frac{1}{4}$ in the intermediate-time regime.

PACS number(s): 47.20.Ky, 47.20.Hw, 05.40.+j, 47.25.Qv

I. INTRODUCTION

Convective instabilities in liquid systems provide an interesting example of nonlinear, nonequilibrium processes. An example of such phenomena that has received considerable attention in recent years is the onset and formation of roll patterns in Rayleigh-Bénard convection [1–16]. In this paper we consider a simple model of this process, the Swift-Hohenberg [1] (SH) equation, to study the situation in which a nonconvective state is brought above the convective threshold for a system of infinite horizontal dimension. Once above the convective threshold, a complex pattern of convective rolls emerges. By studying extremely large systems, we focus our attention on the collective behavior of a large number of rolls. If all sources of fluctuations are small (let F denote their amplitude) the rolls form small locally ordered domains (defined by regions of rolls with the same orientation) that later reorient to become parallel to rolls of larger domains in their immediate vicinity. Dynamic scaling relationships analogous to those found in spinodal decomposition are used to understand the transient dynamics of the collective ordering, while ideas based on critical phenomena are used to analyze the asymptotic steady states.

The SH equation was developed by considering the set of equations for a simple fluid in the Boussinesq approximation, bounded by two infinite horizontal plates separated by a distance d, at temperatures T_1 and $T_1 + \Delta T$, respectively. For values of the Rayleigh number R larger than a critical Rayleigh number R_c, an instability occurs giving rise to convective rolls. The solution of the linearized equations for the velocity field perpendicular to the plates v_z, and for the temperature field θ (or more precisely for the deviations from a linear temperature gradient between the plates) contains stable and unstable eigenvalues. The SH equation is obtained by neglecting all terms proportional to the stable mode and by considering only the wavelengths near the most unstable wavelength obtained in the linear analysis. The SH equation is asymptotically correct in the limit $R \to R_c$. In dimensionless units, the SH equation reads

$$\frac{\partial\psi(\mathbf{r},t)}{\partial t} = \left[\epsilon - \left(1+\nabla^2\right)^2\right]\psi(\mathbf{r},t) - \psi^3(\mathbf{r},t) + \eta(\mathbf{r},t), \tag{1}$$

where ψ is a scalar, two-dimensional field related to the amplitude of the eigenfunction corresponding to the unstable mode and is commensurate with the convective rolls. The quantity $\epsilon = (R - R_c)/R_c$ acts as a control parameter, and η is a random field that follows a Gaussian distribution, with zero mean and correlations,

$$\langle\eta(\mathbf{r},t)\eta(\mathbf{r}',t')\rangle = 2F\delta(\mathbf{r}-\mathbf{r}')\delta(t-t'), \tag{2}$$

where F is the intensity of the noise.

The salient feature of the SH equation is that the Lyapunov functional associated with Eq. (1) is minimized by a one-dimensional periodic function which corresponds to a configuration comprised of straight, parallel rolls. The appearance of such "striped" patterns is a common feature in nature and has also been observed in magnetic films, block copolymers, the visual cortex, liquid crystals, microemulsions, and eutectic growth. Equation (1) can be expressed in terms of a Lyapunov functional $\mathcal{F}$ in the following manner:

$$\frac{\partial\psi(\mathbf{r},t)}{\partial t} = -\frac{\delta\mathcal{F}(\psi)}{\delta\psi(\mathbf{r},t)} + \eta(\mathbf{r},t), \tag{3}$$

where $\mathcal{F}$ is given by

$$\mathcal{F} = \int d\mathbf{r}\left\{-\psi\left[\epsilon - \left(1+\nabla^2\right)^2\right]\psi/2 + \psi^4/4\right\}. \tag{4}$$

As noted in the original work of Swift and Hohenberg [1], this model does not fall within the classification scheme of Halperin and Hohenberg [17]. Although other systems select a characteristic wavelength which is finite (as in order-disorder or antiferromagnetic transitions), this model differs in that the pattern of rolls is rotationally invariant. Thus small changes in orientation are associated with very small changes of $\mathcal{F}$. Another important feature of Eq. (3) is that ψ is a nonconserved variable since $\int d\mathbf{r}\,\psi(\mathbf{r},t)$ can vary in time. In Sec. II a Lyapunov functional with these two generic properties is considered, in order to both study the SH equation and to establish the extent to which our work may apply to other systems.

For the one-dimensional SH equation, Pomeau and Manneville [7] have obtained an approximate solution $\psi^{d=1}$ that minimizes $\mathcal{F}$ in the limit of small ϵ. This solution will be used to estimate the size of various quantities that enter into the analytic calculation given in Sec. II. The solution is given in a power series in ϵ, and is

$$\psi^{d=1}(x) = \sum_{i=0}^{\infty} a_i \sin\left(k_0\left[2i+1\right]x\right), \tag{5}$$

where $a_0(k_0) = \sqrt{4\omega(k_0)/3}$, $a_1(k_0) = -a_0(k_0)^3/4\omega(3k_0)$, $\omega(k_0) = \epsilon - (1-k_0^2)^2$, and $k_0 = 1 - \epsilon^2/1024$. In two dimensions, a solution that minimizes $\mathcal{F}$ is, for example, $\psi(x,y) = \psi^{d=1}(x)$. This solution corresponds to a set of straight rolls parallel to the y direction. Although this solution minimizes $\mathcal{F}$, it is doubtful that it could be obtained via numerical simulation of the SH equation from an initially random state due to the difficulty in removing defects in the absence of fluctuations. In fact, Pomeau and Zaleski [8], and Kramer and Zimmermann [9] have derived other stationary solutions to the one-dimensional SH equation that are not a global minimum of $\mathcal{F}$ and involve a local shift in the phase of ψ [e.g., $\psi\sin(k_o x)$ for $x < -a$ and $\psi\sin(k_o x+\pi)$ for $x > a$].

The presence of fluctuations (i.e., $F \neq 0$) changes matters significantly. In one dimension long-range order is broken. A numerical solution of the stochastic SH equation in one dimension by Viñals *et al.* [14] has shown that a finite F leads to a diffuse peak in the structure factor. This one-dimensional result has important implications for the two-dimensional stationary state. If the two-dimensional stationary state is a set of parallel rolls, then no long-range translational order can exist, since the one-dimensional solution should be valid normal to the rolls. The two-dimensional equilibrium state could still, however, exhibit long-range orientational order. One interesting feature of the SH equation is that the orientational order parameter (i.e., a vector that lies normal to the convective rolls) is continuous, similar to the spin field in the XY model. Since the XY model is the prototypical model of a Kosterlitz-Thouless (KT) [18] transition it is possible that the SH model contains such a Kosterlitz-Thouless phase. In fact Toner and Nelson [11, 12] have suggested that this could be the case. In Secs. II and III a more detailed discussion of the stationary states will be presented.

The dynamic evolution to the stationary states is realized through the enlargement of regions of convective rolls with the same orientation and the elimination of defects. A singular perturbation solution [3] to the SH equation predicts that correlations in ψ obey the following scaling relationship:

$$S(k,t) = t^x f([k-k_0]t^x), \tag{6}$$

where $S(k,t) = \sum_{\hat{k}}\langle|\psi(\mathbf{k},t)|^2\rangle/\sum_{\hat{k}}$, k is the wave vector, x is a dynamic scaling exponent, and the orientation of $\hat{k}$ has been averaged over. This relationship should be valid for extremely large systems, comprised of many domains of different orientation. Equation (6) is analogous to the scaling relationships observed in spinodal decomposition and order-disorder transitions. In domain growth phenomena the structure factor has been found to obey the following dynamic scaling relationship [19, 20], $S(k,t) = [R(t)]^d f(kR(t))$, where $R(t) \propto t^x$ is the average domain size and d is the dimension of the system. The differences between this result and Eq. (6) are due to the existence of a nonscaling length: the roll width. The specific value of x has been shown to be of considerable importance in first-order phase transitions, and is particular to a given universality class. Systems with a conserved or nonconserved scalar order parameter fall into classes characterized by $x = \frac{1}{3}$ and $\frac{1}{2}$, respectively.

In Secs. II and III analytic and numerical methods are used to estimate the dynamic exponent x for the SH equation. The analytic calculation is an expansion around a curved set of rolls of varying width, and is an extension of the interfacial methods used in first-order phase transitions. Some of the results of Toner and Nelson [11, 12] alluded to in the preceding paragraph are recovered in Sec. II, and are shown to be consistent with the numerical results given in Sec. III. In the final section a discussion of these results is presented and comparisons with other systems are made.

II. DYNAMICS OF CURVED ROLLS

Insight into the ordering dynamics can be obtained by considering the relaxation of a set of convective rolls in which the orientation and spacing varies slowly in space. This description precludes the explicit consideration of defects, which will be discussed later. A typical pattern that falls within this description is shown in Fig. 1 which was taken directly from the numerical calculations to follow. In the absence of defects, the dynamic evolution can roughly be separated into three distinct mechanisms: the relaxation of the local curvature of the rolls, the relaxation of the distance between consecutive rolls, and the relaxation in the functional form of ψ (to be described later). The latter fluctuations will be seen to decay much faster than the other mechanisms which describe changes in the positions of the rolls. To begin the calculation, a

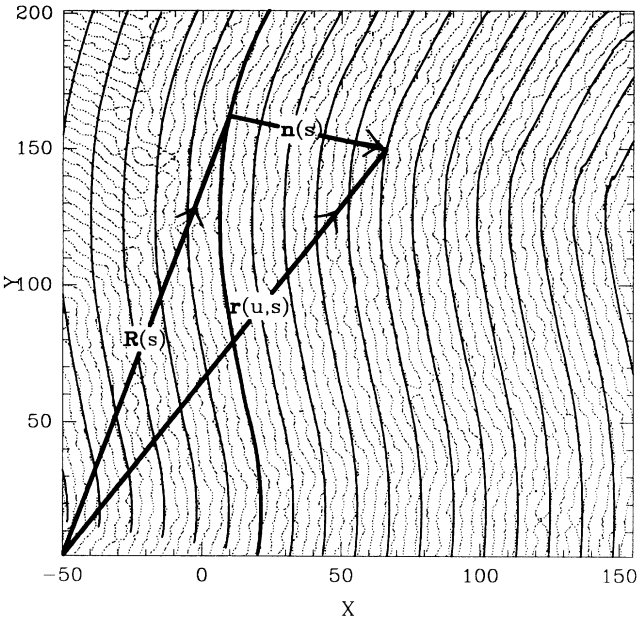

FIG. 1. Curvlinear coordinate system. The dotted lines on this figure are zeros of ψ at $t = 10^4$ for $\epsilon = 0.25$ and $F' = 0.05$. The thick solid line was fit to a particular line defined by $\psi = 0$. The thin lines were calculated by the equation $\mathbf{r} = \mathbf{R} + m\pi/k_0\hat{n}$, where $\mathbf{R}$ is the position of the thick solid line, $\hat{n}$ is the normal to the solid line, and $m = \pm 1, \pm 2, \ldots$.

Lyapunov functional $\mathcal{F}\{\psi\}$ of a scalar function ψ of the form

$$\mathcal{F}\{\psi\} = \int d\mathbf{r}\{-\psi[f(\nabla^2)]\psi/2 + g(\psi)\} \tag{7}$$

is considered, with the restrictions that $\mathcal{F}$ is minimized (in the absence of noise) by a roll structure with characteristic wave number k_0, ψ is nonconserved, and g is an even function of ψ. Subject to these restrictions, the functions f and g can be written $f = \sum_{i=0} a_i(\nabla^2)^i$ and $g = \sum_{i=1} c_i(\psi^2)^{i+1}$. The SH equation can be recovered by choosing $a_0 = \epsilon - 1, a_1 = -2, a_2 = -1$, and $a_{i>3} = 0$, and $c_1 = \frac{1}{4}$ and $c_{i>1} = 0$. We restrict our analysis to even powers of ψ due to the symmetry of roll patterns while pointing out that odd powers of ψ can lead to interesting behavior such as stationary solutions with hexagonal symmetry. The dynamical evolution of ψ is given by

$$\frac{\partial\psi}{\partial t} = -\frac{\delta\mathcal{F}}{\delta\psi} + \eta(\mathbf{r},t) = f(\nabla^2)\psi - \frac{\delta g}{\delta\psi} + \eta(\mathbf{r},t). \tag{8}$$

Other systems that are modeled by Eqs. (7) and (8) include pattern formation in the visual cortex [21] and a model of uniaxial ferromagnetic films [22].

In order to describe the relaxation of the configuration illustrated in Fig. 1, the Cartesian coordinates x and y are mapped onto curvilinear coordinates u and s as indicated in the figure. In this new coordinate system, a vector $\mathbf{r}(x,y) = x\hat{x} + y\hat{y}$ becomes $\mathbf{r}_m(s,u) = \mathbf{R}_m(s) + (u_m - 2m\pi/k_0)\hat{n}_m(s)$, where $\mathbf{R}_m(s)$ is the location of the mth roll, $\hat{n}_m(s)$ is the normal to the mth roll, u_m is restricted to the region $(2m-1)\pi/k_0 < u < (2m+1)\pi/k_0$, and $m = 0, \pm 1, \pm 2, \ldots$. The coordinate system is shown in Fig. 1. In the new coordinates, the Laplacian operator becomes

$$\begin{aligned}\nabla^2 = {} & \frac{\partial^2}{\partial u^2} + \frac{\kappa}{[1+(u_m - m\pi/k_0)\kappa]}\frac{\partial}{\partial u} \\ & + \frac{1}{[1+(u_m - m\pi/k_0)\kappa]^2}\frac{\partial^2}{\partial s^2} \\ & - \frac{(u_m - m\pi/k_0)\kappa_s}{[1+(u_m - m\pi/k_0)\kappa]^3}\frac{\partial}{\partial s},\end{aligned} \tag{9}$$

where the curvature $\kappa = -\partial\theta(s)/\partial s$, $\kappa_s = \partial\kappa/\partial s$, and $\theta(s)$ is the angle between the tangent to the $u_m = 2m\pi/k_0$ curve and the x axis. Assuming that the curvature of all the individual rolls is small, i.e., $\pi\kappa/k_0 \ll 1$, Eq. (9) becomes

$$\nabla^2 \approx \frac{\partial^2}{\partial u^2} + \kappa\frac{\partial}{\partial u} + \frac{\partial^2}{\partial s^2}. \tag{10}$$

Coupling between rolls is incorporated by considering the fluctuations in the separation between them. The field ψ is expanded around the one-dimensional stationary solution in the following manner:

$$\psi(\mathbf{r},t) = \psi^{d=1}[u_m(\mathbf{r},t) + h(u_m,t)] + \delta\psi(\mathbf{r},t), \tag{11}$$

where $\psi^{d=1}$ is defined by the equation

$$f\left(\frac{\partial^2}{\partial u^2}\right)\psi^{d=1} - \left.\frac{\delta g(\psi)}{\delta\psi}\right|_{\psi^{d=1}} = 0. \tag{12}$$

This decomposition describes the relaxation of the local curvature through the curvature dependence of the Laplacian [Eq. (10)], and the relaxation of the separation between rolls through the function h. $\delta\psi$ takes into account fluctuations about the one-dimensional functional form of ψ described by Eq. (12). The validity of this expansion depends on the assumption that the one-dimensional solution $\psi^{d=1}$ is valid normal to the lines defined by $\psi = 0$. The numerical results to follow verify that this is quite a good approximation at late times. As can be seen in Fig. 1, $\psi^{d=1}$ is found to be a good approximation to ψ in the direction normal to the rolls for distances of 6 to 20 consecutive wavelengths. The assumption that h is small precludes a rapid change in the phase of ψ that would be associated with defects.

We next substitute Eqs. (10) and (11) into Eq. (8), and expand to lowest order in κ, h, $\delta\psi$, and their derivatives. This gives the result

$$\begin{aligned}\left(\frac{\partial\psi^{d=1}}{\partial w}\right)\left(\frac{\partial w}{\partial t}\right) + \left(\frac{\partial\delta\psi}{\partial t}\right) = {} & \kappa\sum_{i=1}^{\infty} i a_i \left(\frac{\partial}{\partial w}\right)^{2i-1}\psi^{d=1} + \kappa_{ss}\sum_{i=2}^{\infty}\frac{i(i-1)}{2!}a_i\left(\frac{\partial}{\partial w}\right)^{2i-3}\psi^{d=1} \\ & + \frac{\partial h}{\partial u}\sum_{i=1}^{\infty}(2i)a_i\left(\frac{\partial}{\partial w}\right)^{2i}\psi^{d=1} + \frac{\partial^2 h}{\partial u^2}\sum_{i=1}^{\infty}\frac{(2i)(2i-1)}{2!}a_i\left(\frac{\partial}{\partial w}\right)^{2i-1}\psi^{d=1} \\ & - \left[\left(\frac{\delta^2\mathcal{F}}{\delta\psi^2}\right)\Big|_{\psi=\psi^{d=1}}\right]\delta\psi + \eta + \cdots ,\end{aligned} \tag{13}$$

where $w = u_m + h(u_m)$. The coefficients of the terms proportional to κ and $\partial h/\partial u$ are identically zero if $\psi^{d=1}$ is of the form $\sin(k_0 w)$ or $\cos(k_0 w)$ with k_0 defined by $[\partial f(k)/\partial k]|_{k=k_0} = 0$. For the SH equation, replacing $\psi^{d=1}$ by a sinusoidal function is an extremely good approximation for small ϵ as was shown by Pomeau and Manneville [7]. The coefficient of the term proportional to $\delta\psi$ is less than zero since $\psi^{d=1}$ is a minimum of $\mathcal{F}$ which implies $(\delta^2\mathcal{F}/\delta\psi^2)_{\psi=\psi^{d=1}} > 0$.

The evolution of $\delta\psi$ can be obtained by introducing the projection operator,

$$\mathcal{P}_H \equiv k_o/(2\pi)\int_{(2m-1)\pi/k_0}^{(2m+1)\pi/k_0} dw.$$

Applying $\mathcal{P}_H$ to Eq. (13) gives

$$\frac{\partial\delta\psi}{\partial t} = \left[f(\nabla^2) - \mathcal{P}_H\left(\frac{\delta^2 g(\psi)}{\delta\psi^2}\right)\Big|_{\psi=\psi^{d=1}}\right]\delta\psi + \eta', \quad (14)$$

where

$$\langle\eta'(n,s_1,t_1)\eta'(m,s_2,t_2)\rangle = 2F[\delta_{n,m}/(2\pi/k_0)]\delta(s_1-s_2)\delta(t_1-t_2).$$

In deriving this equation, it was explicitly assumed that the length scale over which $\delta\psi$ varies is much greater than the roll wavelength; that is, $\delta\psi$ is approximately constant over length scales of the order $2\pi/k_0$. In addition it was assumed that the coefficient of $\partial h/\partial u$ was negligible. For the SH equation, Eq. (14) becomes

$$\frac{\partial\delta\psi}{\partial t} = [-2\epsilon - (1+\nabla^2)^2]\delta\psi + \eta', \quad (15)$$

if Eq. (5) to lowest order in ϵ is used for $\psi^{d=1}$. Thus $\delta\psi$ decays exponentially in time since $-2\epsilon-(1-k^2)^2$ is less than zero for all k. In the next few paragraphs, it will be shown that the other mechanisms decay as a power law in time and, consequently, the relaxation of the initial roll pattern considered is controlled by the motion of the rolls.

These dynamics can be extracted by applying a different projection operator, i.e.,

$$\mathcal{P}_P \equiv k_o/(2\pi)\int_{(2m-1)\pi/k_0}^{(2m+1)\pi/k_0} dw\left(\frac{\partial\psi^{d=1}}{\partial w}\right).$$

Applying $\mathcal{P}_P$ to Eq. (13) gives

$$\frac{\partial w}{\partial t} = b_1\kappa + b_2\kappa_{ss} + b_3\frac{\partial^2 h}{\partial u^2} + \zeta(u,s,t), \quad (16)$$

where

$$b_1 = \sum_{i=1}^{\infty} i a_i \frac{\sigma_{2i-1}}{\sigma_1}, \quad (17)$$

$$b_2 = \sum_{i=2}^{\infty} a_i \frac{i(i-1)}{2!}\frac{\sigma_{2i-3}}{\sigma_1}, \quad (18)$$

$$b_3 = \sum_{i=1}^{\infty} a_i \frac{(2i)(2i-1)}{2!}\frac{\sigma_{2i-1}}{\sigma_1}, \quad (19)$$

$$\sigma_i = k_o/(2\pi)\int_{(2m-1)\pi/k_0}^{(2m+1)\pi/k_0} dw\left(\frac{\partial\psi^{d=1}}{\partial w}\right)\left(\frac{\partial^i\psi^{d=1}}{\partial w^i}\right), \quad (20)$$

and

$$\langle\zeta(m,s,t)\zeta(n,s',t')\rangle = (2F/\sigma_1)[\delta_{m,n}/(2\pi/k_0)]\delta(s-s')\delta(t-t').$$

Equation (16) is the main result of this calculation. A simple dimensional analysis of Eq. (16) reveals that two different mechanisms provide different relaxational rates: The distance between rolls relaxes at a rate of $t^{-1/2}$, while the curvature of the rolls relaxes at a rate of $b_1 t^{-1/2} + b_2 t^{-1/4}$. If $\psi^{d=1} = A\sin(k_0 u)$, then the coefficient b_1 is identically zero, and the rolls straighten at a rate of $t^{-1/4}$, which is considerably slower than the relaxation of the fluctuations in the distance between rolls. Therefore curvature relaxation is the dominant mechanism in the limit $b_1 = 0$. Corrections to a sinusoidal $\psi^{d=1}$ are generally small close to onset. This leads to a small but finite value of b_1 (e.g., for $\epsilon = 0.25$, $b_1 \approx 1.0\times10^{-3}$). The low value of b_1 indicates that the asymptotic behavior in which the curvature relaxes with a single power law with an exponent of $\frac{1}{2}$ should not be expected until very late times. To estimate the time at which the crossover from an exponent of $\frac{1}{4}$ to $\frac{1}{2}$ occurs it is useful to determine the dynamics of the line defined by $w(x,y,t) = 0$, i.e., $\mathbf{r} = x\hat{x} + y(x,t)\hat{y}$. In this calculation we consider only the effect of curvature and consequently drop the term proportional to b_3 and the noise term. The growth exponent can be inferred by the rate of relaxation of the deviations (ΔS) of the arc length from its asymptotic value L, i.e., $\Delta S = L - \int_0^L dx\sqrt{1+(y')^2}$. To lowest order in $(dy/dx)^2$ and for L large, ΔS becomes,

$$\Delta S(t) \approx (C^2\sqrt{b_1/|b_2|}/8)e^{b_1^2 t/4|b_2|}K_{1/4}(b_1^2 t/4|b_2|) \rightarrow C^2\sqrt{\pi/(8b_1)}t^{-1/2} \quad (t\rightarrow\infty) \quad (21)$$

where $K_{1/4}$ is the Bessel function of an imaginary argument and random fluctuations (of amplitude C) were chosen for the dimensionless quantity $y'(x,t=0)$. $\Delta S(t)$ is plotted as a function of time in a latter figure [i.e., see the inset in Fig. 8(b)] and shows that the crossover to the $\frac{1}{2}$ exponent does not occur until $t \approx 10^6 - 10^7$.

Equation (16) also describes the local fluctuations in the position of the rolls. If the magnitude of the noise intensity (i.e., $2F/\sigma_1$) is sufficiently strong, i.e., greater than the distance between the rolls, the pattern of parallel rolls would be broken. Hence a transition to a disordered state will occur when $F_{\mathrm{KT}} \propto \sigma_1/k_0^2$ (for the SH equation this corresponds to $F_{\mathrm{KT}} \propto \epsilon$). It should be noted that σ_1 is typically proportional to k_0^2. The constant of proportionality is difficult to obtain; moreover, it would depend on the existence of defects.

The effect of defects in related models has been studied by Toner and Nelson [11, 12]. Their analysis begins with a generic free energy of the form

$$G(w) \equiv (B/2) \int d\mathbf{r} \left[\left(\frac{\partial w}{\partial y} \right)^2 + \lambda^2 \left(\frac{\partial w^2}{\partial x^2} \right)^2 \right]. \quad (22)$$

Assuming that b_1 is negligible, Eq. (16) can be written in the form

$$\frac{\partial w(x,y,t)}{\partial t} \approx -\frac{\delta G(w)}{\delta w} + \zeta, \quad (23)$$

where the free energy $G(w)$ is given by Eq. (22), with $B = b_3$ and $\lambda^2 = -b_2/b_3$. Toner and Nelson [11, 12] have shown that defects in conjunction with the generic free energy given in Eq. (22) leads to algebraic decay in the orientational correlation function $(C(r))$, i.e., $C(r) = \langle e^{2i\phi(\mathbf{r})} e^{2i\phi(0)} \rangle \approx |\mathbf{r}|^{-v}$, where $\phi \equiv -\partial w/\partial x$ and [26] $v = -2F/(\pi b_2 \sigma_1)$. The algebraic decay with distance with an F-dependent exponent implies that the state is a Kosterlitz-Thouless phase. By using the theory of Kosterlitz and Thouless [18] a transition to a disordered state occurs when $v = \frac{1}{4}$ or $F_{\rm KT} = -\pi b_2 \sigma_1/8$. For the SH equation [assuming $\psi^{d=1} = \sqrt{4\epsilon/3}\sin(w)$] this relationship becomes $F_{\rm KT} = \pi\epsilon/12$. If an analogy with liquid crystals can be made, as suggested by Toner and Nelson [11, 12], various phases can be identified: an *isotropic* phase (for $F > F_{\rm KT}$), a *nematic* or Kosterlitz-Thouless phase (for $0 < F < F_{\rm KT}$), and a *smectic* phase (at $F = 0$). In using this terminology, we are explicitly following the somewhat unconventional terminology of Toner and Nelson's [11, 12] two-dimensional melting picture of liquid crystals. For the purpose of this paper, we use the term *isotropic* to refer to a system with short-range order, the term *nematic* to describe a system with quasi-long-range orientational order, and *smectic* to refer to a phase with long-range orientational and translation order. In this terminology all phases select a finite wavelength, as can be seen in Fig. 2, which depicts portions of typical final configurations obtained by numerical simulations of Eq. (1) along with the phase diagram. It should be noted that the configurations labeled *nematic* and *smectic* have not reached a stationary state and consequently the labels correspond to the analytic results given above. An implication of these results is that in order to observe a scaling relationship an orientational correlation function should be measured; however, $S(k,t)$ should provide an accurate description of the ordering dynamics when the translational correlation length is larger than the average domain size.

The results of the preceding paragraphs indicate that the dynamics in the absence of defects is controlled by the straightening of rolls, and the rate associated with this mechanism is $t^{-1/4}$ during an intermediate time regime. The effect of defects on the dynamics has been considered for a similar model (the XY model) by Kawasaki [23] and Loft and DeGrand [24]. Dimensional arguments and numerical simulations of the XY model led Kawasaki [23] and Loft and DeGrand [24], respectively, to the conclusion that the separate mechanism of defect recombination occurs at a rate of $t^{-1/2}$. If the annealing away

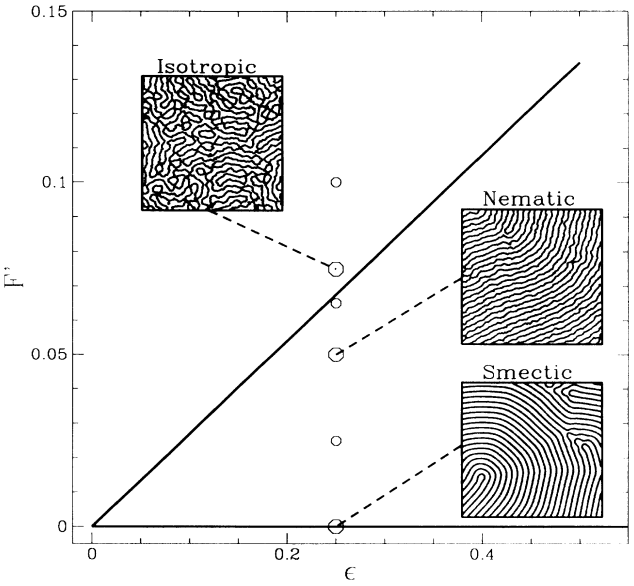

FIG. 2. Portions of size 100 × 100 of typical configurations obtained. The large and small circles correspond to the large and small (see text) numerical simulations conducted at $F' = 0.075$, 0.05, and 0, and $F' = 0.025, 0.065$, and 0.1, respectively. The configurations shown in the insets labeled isotropic, nematic, and smectic correspond to $F' = 0.075$, 0.05, and 0. The nematic and smectic configurations are shown at $t = 10^4$ and are still evolving in time. In the insets the lines shown are for $\psi(\mathbf{r}) = 0$. The thick solid line represents the numerical transition line, $F' = 0.27\epsilon$.

of defects in the SH equation is the same as in the XY model, then the curvature relaxation mechanism should still dominate in the intermediate-time regime since it is the slower mechanism. The expected crossover to $x = \frac{1}{2}$ at late times might, however, be influenced by defects. The more important influence of defects is the breaking of translational order and the creation of a disordered state above $F_{\rm KT}$.

The idea of expanding ψ around an almost parallel roll configuration has been used by others, including Toner and Nelson [12] and Ahlers *et al.* [10]. In these works $\psi(x,y)$ is expanded around $\sin(k_0 x)$, not in a coordinate system commensurate with the curved rolls. Cross and Newell [15] considered a perturbative expansion of the complex SH equation. The leading-order term in this expansion is sinusoidal, but higher-order terms lead to results that are somewhat similar to ours in that curvature is identified as playing an important role in the dynamics. While the above techniques have provided much insight into the SH equation, the projection operator method used in this work has several advantages. The method provides insight into both the dynamics and stationary solutions in the presence of noise, without explicit knowledge of the one-dimensional solution (i.e., $\psi^{d=1}$), or the precise details of the free energy. In addition, the projection operator techniques not only decouple fluctuations in the functional form of ψ from curvature and wavelength relaxation, but also show that the fluctuations in

the functional form of ψ are irrelevant, since their decay is extremely fast.

III. NUMERICAL SOLUTION

The numerical results to be presented were obtained by discretizing both space and time derivatives in Eq. (1). Euler's method was used to discretize the time derivative and the approximation for the Laplacian included contributions from nearest and next-nearest neighbors. Schematically the numerical algorithm can be written

$$\psi(i,j,n+1) = \psi(i,j,n) + \Delta t\Big\{(\epsilon - [1+\nabla^2]^2)\psi(i,j,n) - \psi(i,j,n)^3 + \eta(i,j,n)\Big\}, \quad (24)$$

where the indices (i,j) represent the coordinates (x,y) and the index n represents time. The Laplacian is evaluated using the following discrete operator:

$$\nabla^2\psi(i,j) = \left(\tfrac{1}{4}\sum_{(\mathrm{NN})} + \tfrac{1}{2}\sum_{(\mathrm{NNN})} - 3\right)\psi(i,j)/(\Delta x)^2, \quad (25)$$

where the notations (NN) and (NNN) refer to the nearest and next-nearest neighbors to the site (i,j), respectively. Absolute time and spatial coordinates are recovered by the simple relationships $t = n\Delta t$ and $\mathbf{r} = (i\hat{x} + j\hat{y})\Delta x$.

As in most numerical simulations of this nature the choice of $(\Delta t, \Delta x)$ is dictated by the conflicting constraints imposed by the need for numerical accuracy and the finite computational power available. The former constraint requires $(\Delta t, \Delta x)$ to be vanishingly small, while the latter requires the opposite. In practical terms the size of Δx is limited by the smallest length scale in the problem. Typically the choice for Δx imposes a restriction on Δt which can be obtained from a linear stability analysis of the discrete map Eq. (24). In some problems there may also exist nonlinear numerical instabilities that further restrict the size of Δt. For the SH equation Δx must be smaller than the wavelength selected, which is of the order 2π. Δx was chosen to be $2\pi/8$ to satisfy this constraint. The linear solution of the discrete map given in Eq. (24) contains a numerical instability (i.e., subharmonic bifurcation) that occurs when

$$\Delta t > \frac{2(\Delta x)^4}{[4-(\Delta x)^2]^2 - \epsilon(\Delta x)^4}. \quad (26)$$

Thus to avoid numerical instability in the linear analysis for $\epsilon = 0.25$ and $\Delta x = 2\pi/8$, Δt must be less than 0.067 (for the standard nearest-neighbor discrete Laplacian operator Δt should be less than 0.014). Although this analysis does not take into account the noise term or the nonlinear terms, it does provide a minimum requirement. Under these considerations a time step of $\Delta t = 0.05$ was chosen and no numerical instabilities were observed. Test runs with a smaller Δx indicate that the dynamics of $S(k,t)$ are insensitive to decreasing grid size near $k = k_0$ [25]. The bulk of the simulations were run on a 512×512 periodic lattice for $\epsilon = 0.25$ at $F' = 0, 0.05,$ and 0.075 [where $F' = F/(\Delta x)^2$] and averaged over 25 independent runs. Smaller systems were used to examine the dynamics (at $F' = 0.025, 0.065,$ and 0.1) and stationary solutions (at a large number of values F' between 0 and 0.09). For nonzero F', ψ was initially set to zero, while for $F' = 0$, ψ was chosen to be a random variable that follows a Gaussian distribution with zero mean and variance 0.1.

The results of the numerical simulations suggest that there is a qualitatively different behavior between the runs conducted at high and low noise strengths. At high noise strengths a steady state was rapidly reached which corresponded to a disordered structure. Figures 3(a) and 3(b) display the configurations at $t = 2500$ and 10^4, respectively, for $F' = 0.075$. The striking similarity of these configurations and small domain sizes indicates that a disordered stationary state has been achieved. In contrast, at low noise strengths a slow ordering of domains was observed for all times probed. Figures 3(c), 3(d), and 3(e) display the configurations at $t = 10^2$, 10^3, and 10^4, respectively, for $F' = 0.05$. A similar time sequence is shown for $F' = 0$ in Figs. 3(f), 3(g), and 3(h). It is important to note that these runs had not reached a steady state as the rolls were continuing to order. The pronounced difference between the low and high noise strength simulations was also apparent in the structure factors and one-point distribution function $\rho(\psi)$. In Fig. 4(a) $S(k, t = 700)$ is shown for $F' = 0.075$. This structure factor was statistically indistinguishable from any $S(k,t)$ past $t = 200$. The solid line in this figure is a fit to $A/[B + (k^2 - k_0^2)^2]$, which is suggestive of a disordered phase. The structure factors shown in Figs. 4(b) and 4(c) for $F' = 0.05$ and 0, respectively, are significantly different for two reasons. First, their shape is much sharper and, second, they are continuing to evolve in time. Further indication of the qualitative differences is shown in Fig. 5 which compares $\rho(\psi)$ at the latest times for the three noise strengths. The low noise strength one-point distributions are bimodal, while the high noise strength ρ is peaked at $\psi = 0$. To obtain an estimate of where the transition occurs at for $\epsilon = 0.25$, a stationary solution at $F' = 0.09$ was obtained and then F' was decremented in steps of 0.005 at time intervals of 10^3. This test reveals a transition in the region $F'_{\mathrm{KT}} = 0.065 - 0.070$ (or $F' \approx 0.27\epsilon$) which is signaled by a sharp decrease in the peak height of $S(k)$, and a crossover from a bimodal to unimodal distribution in ρ. In Fig. 6 the peak position in ρ is shown as a function of F'. A similar transition has also been observed in parametrically forced surface waves by Gollub and Ramshankar [27]. In these experiments the transition was marked by a dramatic drop in the correlation length and from a crossover from a bimodal to unimodal distribution in ρ.

Although the numerical picture is consistent with the predictions given in Sec. II, it is important to note the limitations of the numerical results. The predictions of smectic, nematic, and disordered states were not unambiguously verified. What is apparent is that the runs above F'_{KT} are disordered states. The numerical results also strongly suggest that the states below F'_{KT} are quali-

tatively different from those above. Indeed, the structure factors for the smectic and nematic simulations were indistinguishable at the latest times. If the $F' = 0.05$ is a nematic state, one should observe only quasi-long-range orientation order. In contrast, the numerical results indicated growth of translational order up until the latest times probed. Thus the numerical results indicate a transition from a disordered state to one with long or quasi-long-range translational order. Presumably, if later times were probed an orientational order parameter would have to be introduced to observe the subsequent ordering of domains. At the very least the transition observed corresponds to one in which there is a dramatic change in translational order at $F'_{\rm KT} \approx 0.0675$.

The dynamics of the collective ordering of rolls was analyzed in terms of the dynamic scaling relationship given in Eq. (6) for $F' < F'_{\rm KT}$. In Figs. 7(a) and 7(b) $S(k,t)$ is displayed for $F' = 0$ and 0.05, respectively, at several times. The ordinate in these plots is $S(k,t)/t^x$ and the abscissa is $(k_0 - k)t^x$. If the scaling predictions are correct, the scaled form of $S(k,t)$ should overlap for all times, near $k = k_0$. For $F' = 0$ [see Fig. 7(a)] the struc-

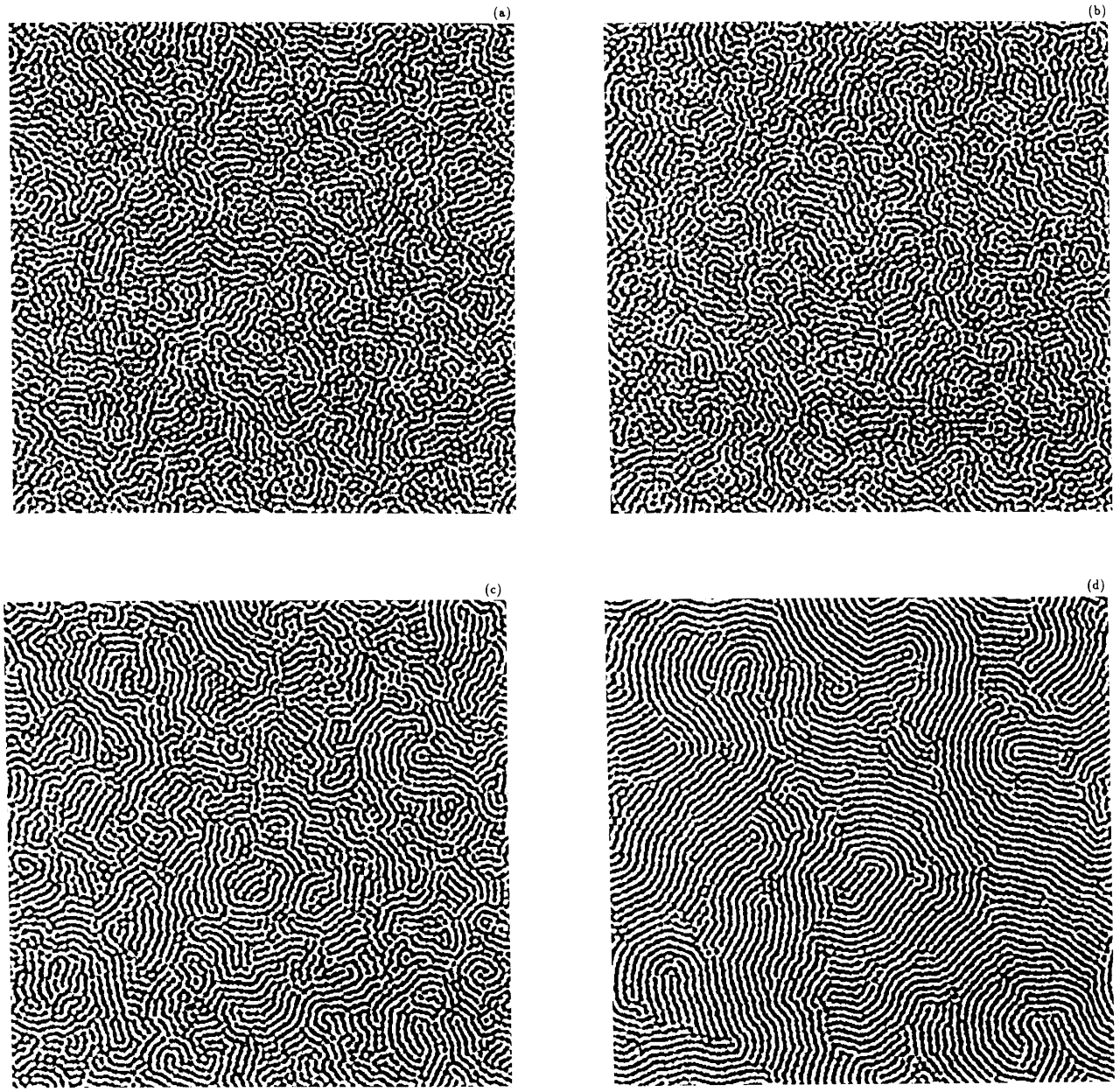

FIG. 3. Sample configurations are displayed for $\epsilon = 0.25$ at various times and noise strengths. In all figures the points correspond to $\psi > 0$. The configurations shown in (a) and (b) correspond to $t = 2500$ and 10^4, respectively, for $F' = 0.075$. In (c), (d), and (e) the configurations correspond to $t = 10^2, 10^3$, and 10^4, respectively, for $F' = 0.05$. A similar time sequence is shown in (f), (g), and (h) for $F' = 0$.

ture factor scales remarkably well over the time range $t = 10^2$ to 10^4, with a growth exponent of $x = \frac{1}{5}$. Figure 7(b) shows that the dynamic scaling hypothesis also works very well for $F' = 0.05$, if a growth exponent of $\frac{1}{4}$ is used. If the scaling hypothesis is valid, all length scales (except the convective roll width) should scale with the same dynamic exponent. To investigate this hypothesis the height (A), width (w), and various moments $m_n(t)$ of $S(k,t)$ were calculated. The height and width were determined by fitting the top portion of $S(k,t)$ to a Gaussian of the form $Ae^{-[(k^2-k_0^2)/w]^2}$ and the moments were defined to be $m_n(t) = \int_{k_0-w(t)}^{k_0+w(t)} dk|k-k_0|^n S(k,t)$. In fitting $S(k,t)$, k_0 was found to be very close to 1 which is the value selected by linear theory. The scaling relationship given in Eq. (6) implies that $m_n(t) \propto t^{-nx}$, $w \propto t^{-x}$, and $A \propto t^x$. The results are shown in Figs. 8(a) and 8(b) for $F' = 0$ and 0.05, respectively. For $F' = 0$ the exponents measured from all lengths scales are within 2% of $\frac{1}{5}$, while the exponents are all within 1% of $\frac{1}{4}$ for $F' = 0.05$. Although the statistics collected for $\epsilon = 0.025$ and 0.065 were not sufficient to obtain accurate values of x, the measured exponents were significantly closer to $\frac{1}{4}$ than $\frac{1}{5}$. Computational restrictions made it impossible to probe the expected crossover to an exponent of $\frac{1}{2}$ at very late times, and consequently no evidence of a crossover was observed.

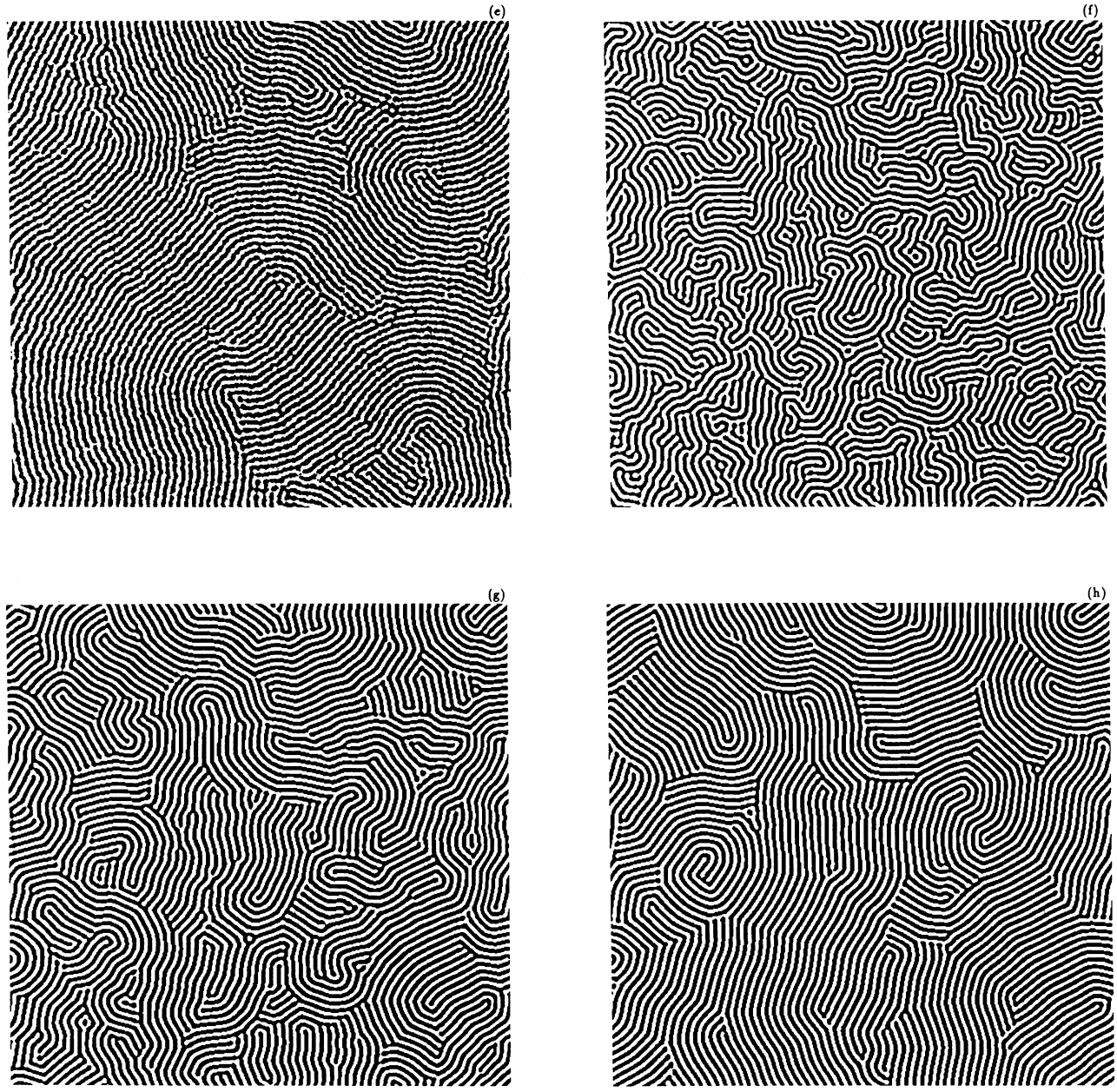

FIG. 3. (*Continued*).

IV. DISCUSSION AND SUMMARY

The results of the numerical and analytic work provide several predictions for the collective ordering of rolls in the limit of infinite aspect ratio. The stationary or steady states should be strongly influenced by any random-noise source, such that above some critical noise strength (i.e., $F_{\rm KT}$) an isotropic state emerges characterized by a diffuse peak in $S(k)$. Below $F_{\rm KT}$ phases with much larger translational correlation lengths emerge. It should be emphasized that the numerical work indicates that the transition is characterized by a drastic increase in translational order, but was not sufficient to determine the precise nature of the states below $F_{\rm KT}$. An independent estimate of the transition line ($F_{\rm KT} \propto \epsilon$) was obtained in Sec. II. Further investigation at other values of ϵ would be useful to establish this relationship. The use of the generic free energy given in Eq. (7) provides insight into the breakdown of periodically ordered systems. In essence the periodicity is broken when the noise

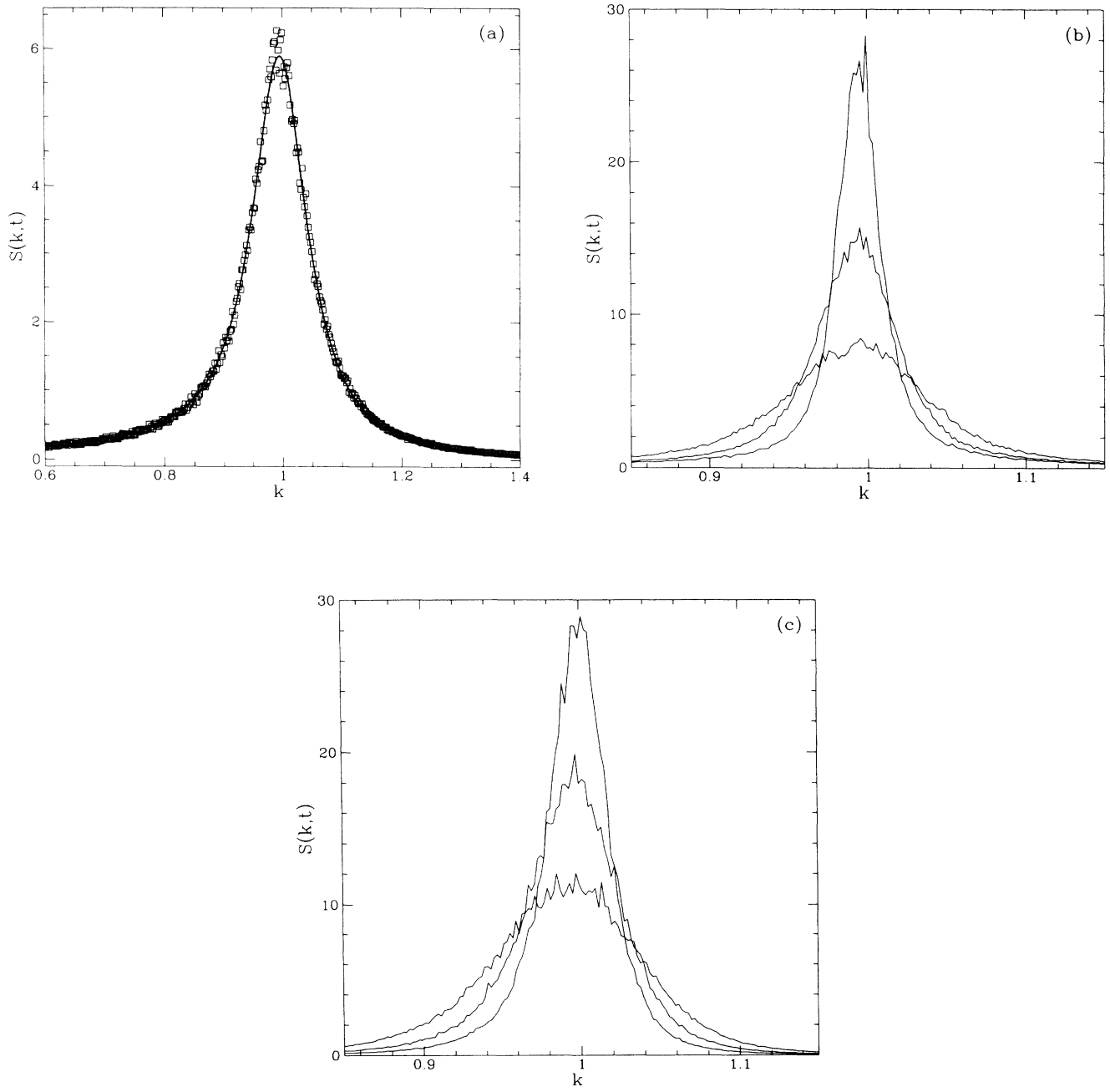

FIG. 4. In (a), $S(k,t)$ is displayed for $F' = 0.075$ at $t = 700$. In this figure the points correspond to the numerical result and the solid line is a fit to $A/[B + (k^2 - k_0^2)^2]$. In (b) and (c), $S(k,t)$ is shown at $F' = 0.05$ and 0.0, respectively. In both these figures, the curves (from bottom to top at $k = 1$) correspond to $t = 10^2$, 10^3, and 10^4. The difference between the high noise strength simulation and the low noise strength simulations can be seen in the scale change between (a) and (b) and (c).

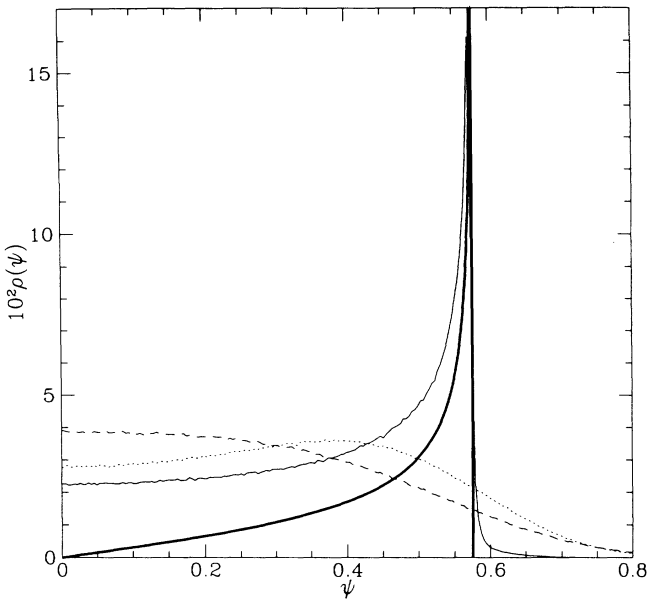

FIG. 5. A comparison of the one-point distribution function for $F' = 0, 0.05$, and 0.075 at $\epsilon = 0.25$. The solid, dotted, and dashed lines correspond to $F' = 0$ at $t = 10^4$, $F' = 0.05$ at $t = 10^4$, and $F' = 0.075$ at $t = 700$, respectively. The thick solid line corresponds to a sine function. It should be noted $\rho(\psi)$ is symmetric about $\psi = 0$ and thus a bimodal distribution produces a peak at a finite ψ in this figure.

strength divided by σ (which is typically proportional to the control parameter causing the instability) is of the order of the wavelength of the periodic structure. The transition observed by Gollub and Ramshankar [27] in parametrically forced surface waves may also be of this nature.

The dynamical behavior of the collective ordering below F_{KT} was found to obey the dynamic scaling relationship given in Eq. (6) for at least three decades in time. In addition, a growth exponent of $x = \frac{1}{4}$ was observed for $0 < F < F_{KT}$. This value of x disagrees with an earlier theoretical calculation and we have presented a possible resolution of the discrepancy. Our calculations show that curvature relaxation leads to an early time exponent of $\frac{1}{4}$ that should eventually crossover to late time exponent of $\frac{1}{2}$. We are, however, unable to explain the smaller

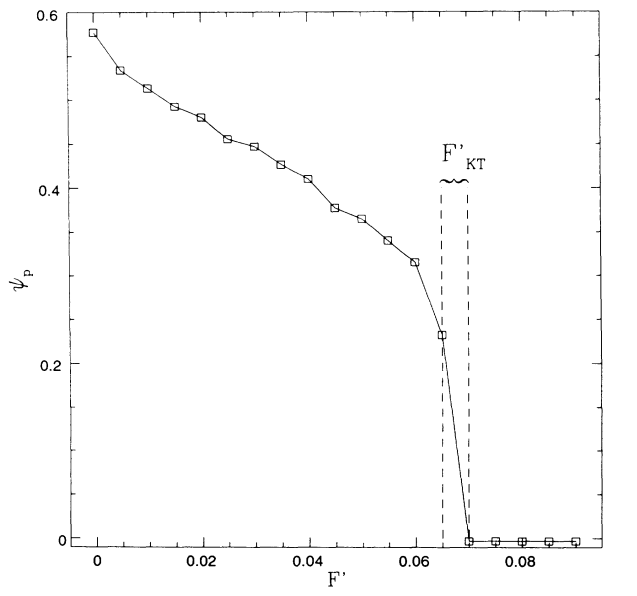

FIG. 6. Position of the peak (ψ_p) in the one-point distribution function ($\rho(\psi)$) as a function of F' for $\epsilon = 0.25$.

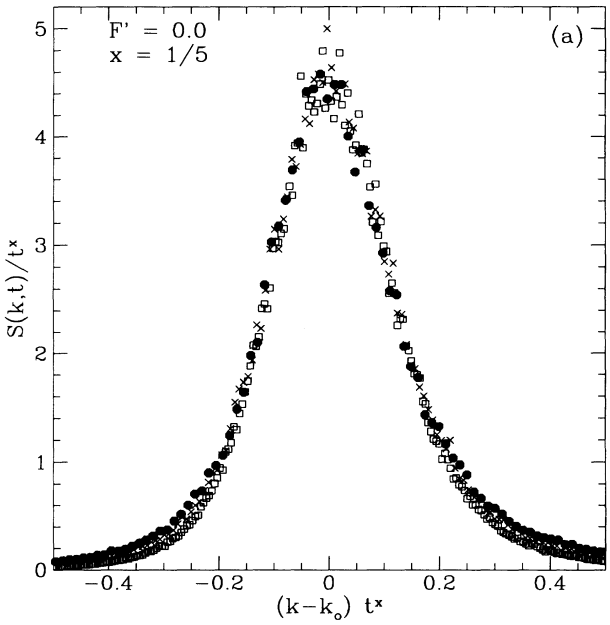

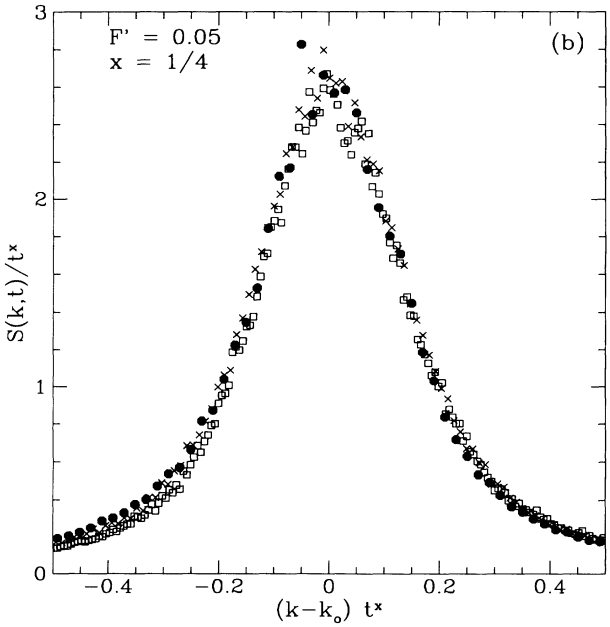

FIG. 7. The dynamic scaling of $S(k,t)$ is shown for $F' = 0$ and 0.05 in (a) and (b), respectively. In both figures the open squares, crosses, and solid circles correspond to $t = 10^2$, 10^4, and 10^5, respectively.

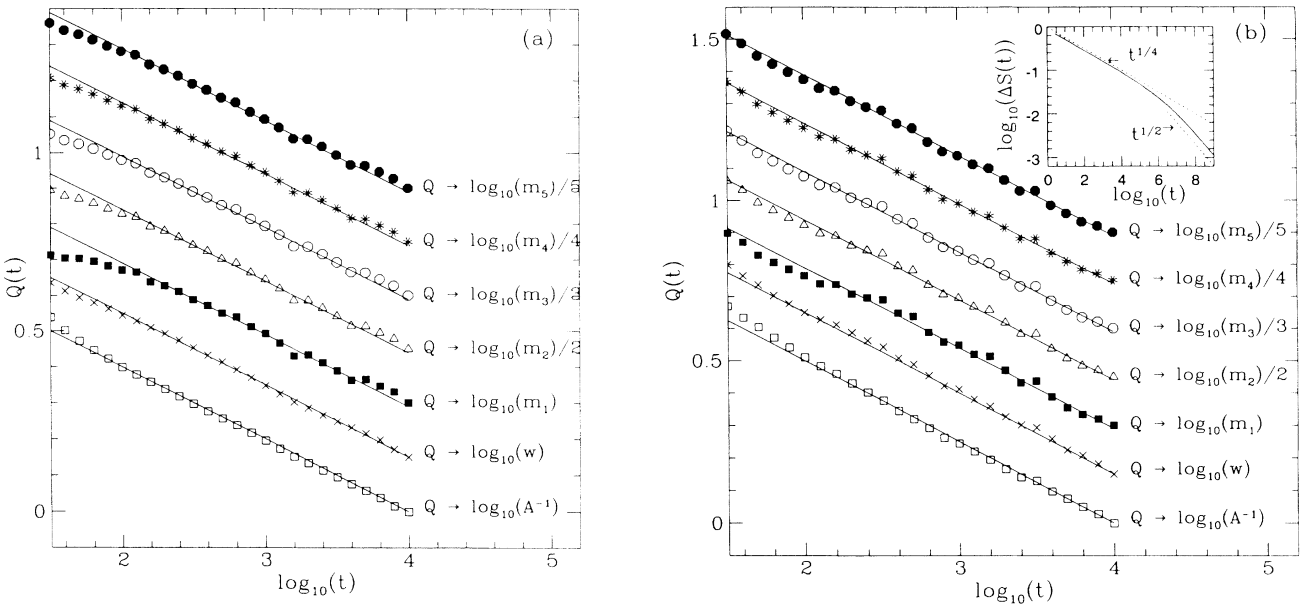

FIG. 8. The amplitude $A(t)$, width $w(t)$, and first five moments $m_n(t)$ of $S(k,t)$ as defined in the text are displayed for $F' = 0$ and 0.05 in (a) and (b), respectively. The solid lines are presented as guides to the eye and all have slope $x = \frac{1}{5}$ in (a) and $x = \frac{1}{4}$ in (b). In the inset of (b), ΔS is plotted on a logarithmic scale for $\epsilon = 0.25$.

exponent of $x = \frac{1}{5}$ observed for $F = 0$. Although this work focused on the stochastic Swift-Hohenberg equation, we expect that both features discussed, namely the existence of a transition from a quasiordered to a disordered state, and the asymptotic dynamical scaling behavior, are generic features of two-dimensional systems defined by Eq. (8).

The difficulty in observing these phenomena in Rayleigh-Bénard experiments is that previous experiments were conducted on very small systems in which boundary effects play an important role. In addition, the noise strengths estimated for real experiments are typically much too small to observe the transition. It is conceivable that external noise sources could be employed to provide large values of F, although to our knowledge this has not been attempted. Recent experimental studies of electrohydrodynamic convection in nematic liquid crystals [28] have been able to detect and quantify the amplitude of the fluctuations before onset. Furthermore, since typical roll widths in these systems are of the order of microns, large-aspect-ratio samples are readily available. However, the pattern that emerges in these systems is strongly anisotropic in that a preferred direction is selected, whereas the equation that we have studied is manifestly isotropic. Another candidate is the recent Rayleigh-Bénard experiments of Bodenschatz *et al.* [16] which employ pressurized gases instead of liquids. In these experiments very large aspect ratios (of the order of 100) have been achieved. These experiments are influenced by non-Boussinesq effects which lead to quadratic terms in ψ in the SH equation. Nevertheless these effects can be small in appropriate experimental conditions. In spite of the mentioned difficulties, we believe it would be of considerable interest to analyze the structure of the steady states, and the transient dynamics following the convective instability in both systems.

ACKNOWLEDGMENTS

This international collaboration has been made possible by a grant from NATO within the program "Chaos, Order and Patterns; Aspects of Nonlinearity," Project No. CRG 890482. This work is also supported by the Natural Sciences and Engineering Research Council of Canada, le Fonds pour las Formation de Chercheurs et l'Aide a la Recherche de la Province de Québec, and by the Supercomputer Computations Research Institute, which is partially funded by the U.S. Department of Energy Contract No. DE-FC05-85ER25000. All the calculations reported here have been performed on the 64 000-node Connection Machine at SCRI. We thank Maxi San Miguel, Mike Kosterlitz, Bertrand Morin, and Emilio Hernández-García for useful discussions.

[1] J. Swift and P.C. Hohenberg, Phys. Rev. A **15**, 319 (1977).
[2] K. Elder, J. Viñals, and M. Grant, Phys. Rev. Lett. **68**, 3024 (1992) gives a preliminary report of these results.
[3] K.R. Elder and M. Grant, J. Phys. A **23**, L803 (1990).
[4] V. Steinberg, G. Ahlers, and D. S. Cannell, Phys. Scr. **T9**, 97 (1984).
[5] C.W. Meyer, G. Ahlers, and D.S. Cannell, Phys. Rev.

Lett. **59**, 1577 (1987).
[6] H. Xi, J. Viñals and J. D. Gunton, Physica A **177**, 356 (1991).
[7] Y. Pomeau and P. Manneville, J. Phys. (Paris) Lett. **23**, L609 (1979).
[8] Y. Pomeau and S. Zaleski, J. Phys. (Paris) **42**, 515 (1981).
[9] L. Kramer and W. Zimmermann, Physica D **16**, 221 (1985).
[10] G. Ahlers, M. C. Cross, P. C. Hohenberg, and S. Safran, J. Fluid Mech. **110**, 297 (1981).
[11] D.R. Nelson, in *Phase Transitions and Critical Phenomena*, edited by C. Domb and J.L. Lebowitz (Academic, London, 1983), Vol. 7.
[12] J. Toner and D.R. Nelson, Phys. Rev. B **23**, 316 (1981).
[13] H.R. Schober, E. Allroth, K. Schroeder, and H. Muller-Krumbhaar, Phys. Rev. A **33**, 567 (1986).
[14] J. Viñals, E. Hernández-García, M. San Miguel, and R. Toral, Phys. Rev. A **44**, 1123 (1991).
[15] M. C. Cross and A. C. Newell, Physica D **10**, 299 (1984).
[16] E. Bodenschatz, S. Morris, J. de Bruyn, D. Cannell, and G. Ahlers, Phys. Rev. Lett. **67**, 3078 (1991); *Proceedings of the KIT International Workshop on the Physics of Pattern Formation in Complex Dissipative Systems*, edited by S. Kai (World Scientific, Singapore, 1992).
[17] P. C. Hohenberg and B. I. Halperin, Rev. Mod. Phys. **49**, 435 (1977).
[18] J.M. Kosterlitz and D.J. Thouless, J. Phys. C **6**, 1181 (1973).
[19] J.D. Gunton, M. San Miguel, and P.S. Sahni, in *Phase Transitions and Critical Phenomena*, edited by C. Domb and J.L. Lebowitz (Academic, London, 1983), Vol. 8, and references therein.
[20] Y. Oono and S. Puri, Phys. Rev. A **38**, 434 (1988).
[21] J. R. Thomson, Wm. Cowan, K. R. Elder, Ph. Daviet, G. Soga, Z. Zhang, M. Grant, and M. J. Zuckermann, J. Bio. Phys. **18**, 217 (1992).
[22] C. Roland and R. C. Desai, Phys. Rev. B **42**, 6658 (1990).
[23] K. Kawasaki, Phys. Rev. A **31**, 3880 (1985).
[24] R. Loft and T. A. DeGrand, Phys. Rev. B **35**, 8528 (1987).
[25] Smaller grid spacings are needed to have the correct spectrum of fluctuations at large k, but we have seen no appreciable differences in $S(k,t)$ around $k = k_0$ for $F < F_{\rm KT}$. In the disordered region or below threshold a large grid spacing would lead to overestimating the intensity of the fluctuations, as measured, for example, by $\int d\mathbf{r}\, \psi^2(\mathbf{r},t)$.
[26] In order to obtain an estimate of v from Ref. (11) it was assumed that the high-temperature values of the constants K_1 and K_3 could be used.
[27] J.P. Gollub and R. Ramshankar, in *New Perspectives in Turbulence*, edited by S. Orszag and L. Sirovich (Springer-Verlag, Berlin, 1991).
[28] I. Rehberg, S. Rasenat, M. de la Torre, W. Schöpf, F. Hörner, G. Ahlers, and H.R. Brand, Phys. Rev. Lett. **67**, 596 (1991).